tributed to the different nature of the ligands. Thus, in the more covalent silylamides **5** and **6**, the four-coordinate bridging nitrogens may impose a more acute bridging angle because of their approximately tetrahedrally disposed orbitals, which may account for the closer approach of the metals. In contrast, the three-coordinate, approximately planar, bridging boryl or aryloxo ligands, are less likely to impose narrow angles at the bridge. This is because a wider MOM angle is expected for the approximately sp^2-hybridized oxygen. More importantly, perhaps, the M–O bonding is more ionic and is less subject to angular restrictions than that generally associated with covalent bonding. In harmony with the longer M···M separations, magnetic studies of **1** and **2** indicate that there is less coupling between the two metal centers. Thus, the μ values measured for **1** and **2** at 300 K are 4.72 and 3.9 μ_B, respectively whereas the values measured for the dimers $[M\{N(SiMe_3)_2\}_2]_2$ (M = Mn or Fe) are 3.26 and 3.52 μ_B, respectively.[14]

Distortions in the structures of **1** and **2** may be attributed, in large part, to the crowding produced by the bulky ligands. For example, in **1** folding of the Mn_2O_2 core as well as deviations from planarity at the bridging oxygen and metal centers are observed, and it is notable that the bridging and terminal ligands are disposed toward opposite sides of the Mn_2O_2 array so as to avoid steric interference. Similarly, in the case of **2**, although the Fe_2O_2 core is planar, both the iron and oxygen centers are slightly pyramidal. In this case, the bridging and terminal ligands are also oriented so as to give the minimum steric interference.

In summary, the first two homoleptic transition-metal boryloxides have been synthesized and structurally characterized. The structural data indicate that the M–O bonding in these cases is mainly ionic rather than covalent. Unexpectedly, the bonding appears to be very similar to that seen in related metal aryloxides. Further studies will be required to determine if this bonding pattern is preserved in other complexes, especially those of the earlier transition metals.

Acknowledgment. We thank the National Science Foundation and the donors of the Petroleum Research Fund, administered by the American Chemical Society, for financial support.

Supplementary Material Available: Details of the solution of structure **1**, full tables of atom coordinates, bond distances and angles, anisotropic thermal parameters, and hydrogen coordinates, and figures that include the full numbering of the ligand atoms (17 pages); tables of structure factors (41 pages). Ordering information is given on any current masthead page.

Contribution from the Department of Chemistry, University of California, Davis, California 95616

Synthesis and Characterization of the Homoleptic Aryloxides $[M\{O(2,4,6\text{-}t\text{-}Bu_3C_6H_2)\}_2]_2$ (M = Mn, Fe), the Adducts $[Mn(OCPh_3)_2(py)_2]$ and $[Fe(OCPh_3)_2(THF)_2]$, and the Mixed Complex $[Fe\{N(SiMe_3)_2\}\{\mu\text{-}O(2,4,6\text{-}t\text{-}Bu_3C_6H_2)\}]_2$: Evidence for Primarily Ionic M–O Bonding

Ruth A. Bartlett, Jeffrey J. Ellison, Philip P. Power,* and Steven C. Shoner

Received January 29, 1991

The characterization of several aryloxide and alkoxide derivatives of manganese and iron is reported. They were synthesized by treatment of the amides $[M\{N(SiMe_3)_2\}_2]_2$ (M = Mn, Fe) with the appropriate alcohol or phenol, in the presence or absence of donor molecules, to give the title compounds. Thus, the reaction of $[M\{N(SiMe_3)_2\}_2]_2$ (M = Mn, Fe) with 2 equiv of HOMes* (Mes* = 2,4,6-t-$Bu_3C_6H_2$) gave $[Mn(OMes^*)_2]_2$ (**1**) or $[Fe(OMes^*)_2]_2$ (**2**). The intermediate species $[Fe\{N(SiMe_3)_2\}(\mu\text{-}OMes^*)]_2$ (**3**) was isolated by using 1 equiv of HOMes*. The base adducts $Mn(OCPh_3)_2(py)_2$ (**4**) (py = pyridine) and $Fe(OCPh_3)_2(THF)_2$ (**5**) were isolated by treatment of the amide with 2 equiv of $HOCPh_3$ in the presence of the base. The X-ray crystal structures of **1**–**3** show them to be dimers with aryloxide bridging. They were further characterized by IR spectroscopy. Variable-temperature ^1H NMR spectroscopy shows that the bridging is quite strong and in the case of **2** is >15 kcal mol^{-1}. The structures of **4** and **5** have very distorted 4-fold coordination at the metals. In all compounds the M–O bonding appears to be primarily ionic with little evidence for a strong M–O π interaction. Crystal data with Mo Kα (λ = 0.71069 Å) at 130 K: **1**, a = 14.201 (6) Å, b = 28.677 (11) Å, c = 18.515 (8) Å, β = 103.30 (3)°, Z = 4, space group $P2_1/c$, 6851 data with $I > 2\sigma(I)$, R = 0.07; **2**, a = 14.343 (6) Å, b = 27.110 (9)°, c = 21.121 (8) Å, β = 101.51 (3)°, Z = 4, space group $P2_1/c$, 5035 data with $I > 2.5\sigma(I)$, R = 0.77; **3**, a = 10.194 (3) Å, b = 12.376 (6) Å, c = 12.558 (3) Å, α = 74.73 (3)°, β = 65.93 (2)°, γ = 84.61 (3)°, Z = 1 (dimer), space group $P\bar{1}$, 5308 data with $I > 2\sigma(I)$, R = 0.040; **4**, a = 9.613 (3) Å, b = 10.614 (3) Å, c = 21.543 (5) Å, α = 79.88 (2)°, β = 78.70 (2)°, γ = 62.86 (2)°, Z = 2, space group $P\bar{1}$, 4103 data with $I > 2\sigma(I)$, R = 0.077; **5**, a = 19.078 (4) Å, b = 9.562 (3) Å, c = 23.454 (3) Å, β = 119.06 (1)°, Z = 4, space group $C2/c$, 2936 data with $I > 3\sigma(I)$, R = 0.039.

Homoleptic, alkoxide and aryloxide (both designated as –OR) derivatives of the later transition metals have been less intensively studied than their early-metal counterparts.[1-4] While it is true that some alkoxide derivatives of almost every later transition metal have been reported, they are often more difficult to study owing to their extensive association and lower solubility in hydrocarbon solvents.[1] Until recently there were very few structural reports for –OR derivatives of the metals Mn → Cu. The use of sterically crowding hydrocarbon substituents, to reduce the extent of alkoxide bridging, is effecting a rapid change in this interesting area. An early paper[5] showed that the degree of association in $Mn(OR)_2$ derivatives was greatly reduced by using large hydrocarbon groups such as 1-adamantyl (1-Ad), $-CPh_3$, or 2,4,6-t-$Bu_3C_6H_2$ (Mes*). Similarly, the use of the ligand $-OCH(t\text{-}Bu)_2$ allowed the isolation of compounds such as $[Co(OR)_2]_2$ or $[Mn(OR)_2]_3$ and the structural characterization of the salt $[ROH\cdot LiFe(OR)_4]$ (R = $CH(t\text{-}Bu)_2$).[6] In addition, ligands such as $-OC(t\text{-}Bu)_3$, $-OCPh_3$, and $-OC(C_6H_{11})_3$ have afforded the mononuclear salts $[Li_2(THF)_2MnBr_2\{OC(t\text{-}Bu)_3\}_2]$,[7] $[LiMn\{OC(t\text{-}Bu)_3\}_2\{N(SiMe_3)_2\}]$,[7] $[Li(THF)_3Co(Cl)\{OC(t\text{-}Bu)_3\}_2]$,[8] $[Li(THF)_{4,5}][Co\{OC(t\text{-}Bu)_3\}_2\{N(SiMe_3)_2\}]$,[8] and $[LiCo\{OC(t\text{-}Bu)_3\}_2\{N(SiMe_3)_2\}]$,[8] the neutral

(1) Bradley, D. C.; Mehrotra, R. C.; Gaur, D. P. *Metal Alkoxides*; Academic: New York, 1978.
(2) Mehrotra, R. C. *J. Ind. Chem. Soc.* **1982**, *LIX*, 715.
(3) Mehrotra, R. C. *Adv. Inorg. Chem. Radiochem.* **1983**, *26*, 269.
(4) Rothwell, I. P. *Acc. Chem. Res.* **1988**, *21*, 153.
(5) Horvath, B.; Möseler, R.; Horvath, E. G. *Z. Anorg. Allg. Chem.* **1979**, *449*, 41.
(6) Bochmann, M.; Wilkinson, G.; Young, G. B.; Hursthouse, M. B.; Malik, K. M. A. *J. Chem. Soc., Dalton Trans.* **1980**, 1863.
(7) Murray, B. D.; Power, P. P. *J. Am. Chem. Soc.* **1984**, *106*, 7011.
(8) Olmstead, M. M.; Power, P. P.; Sigel, G. *Inorg. Chem.* **1986**, *25*, 1027.

0020-1669/91/1330-2888$02.50/0

Table I. Abridged Summary of Data Collection, Structure Solution, and Refinement Parameters for **1–5**

	1	2	3	4	5
formula	$C_{72}H_{116}O_4Mn_2$	$C_{72}H_{116}O_4Fe_2$	$C_{48}H_{76}N_2O_2Si_4Fe_2$	$C_{48}H_{40}O_2N_2Mn$	$C_{46}H_{46}O_4Fe$
fw	1155.60	1157.42	937.19	731.80	718.72
cryst system	monoclinic *P*	monoclinic *P*	triclinic *P*	triclinic *P*	monoclinic *C*
a, Å	14.201 (6)	14.343 (6)	10.194 (3)	9.613 (3)	19.078 (4)
b, Å	28.677 (11)	27.110 (9)	12.376 (6)	10.614 (3)	9.562 (3)
c, Å	18.515 (8)	21.121 (8)	12.558 (3)	21.543 (5)	23.454 (5)
α, deg			74.73 (3)	79.88 (2)	
β, deg	103.30 (3)	101.51 (3)	65.93 (2)	78.70 (2)	119.06 (1)
γ, deg			84.61 (3)	62.86 (2)	
V, Å^3	7338 (5)	8048 (5)	1395.3 (9)	1909 (1)	3740 (1)
space group	$P2_1/c$	$P2_1/c$	$P\bar{1}$	$P\bar{1}$	$C2/c$
Z	4	4	1	2	4
D_{calc}, g/cm^3	1.08	0.98	1.12	1.27	1.28
linear abs coeff, cm^{-1}	3.74	3.99	6.36	3.71	4.43
2θ range, deg	0–50	0–45	0–55	0–50	0–55
no. of obs reflcns	6851 [$I > 2\sigma(I)$]	5035 [$I > 2.5\sigma(I)$]	5308 [$I > 2\sigma(I)$]	4103 [$I > 2\sigma(I)$]	2936 [$I > 3\sigma(I)$]
no. of variables	839	835	290	478	231
R, R_w	0.070, 0.062	0.077, 0.083	0.046, 0.054	0.077, 0.0723	0.039, 0.042

dimeric compounds $[Co(OCPh_3)_2]_2$[9] and $[Co\{OC(C_6H_{11})\}_2]_2$,[9] and the Lewis base complex $Co(OCPh_3)_2(THF)_2$.[9] The latter report also described the characterization of the related siloxy derivative $[Co(OSiPh_3)_2(THF)]_2$.[9] The structure of the neutral, heteroleptic compound $[Mn(CH_2CMe_2Ph)(\mu\text{-}OMes^*)]_2$ has also been published.[10] Other reports that describe the structure of a number of nickel siloxide complexes, including the bridged dimeric species $[Ni(\eta^3\text{-}C_3H_5)\{\mu\text{-}OSi(t\text{-}Bu)_3\}]_2$, have also appeared.[11] In addition, the synthesis and structural determination of a cobalt derivative of the related boroxide ligand $-OBR_2$ in the form of the complex $[Li_2CoCl_2(OBMes_2)_2]$ has been published.[12]

In this paper the detailed characterization of the neutral homoleptic compounds $[M(OMes^*)_2]_2$ (M = Mn (**1**), Fe (**2**)) is described. In addition, the synthesis and structures of the mixed complex $[Fe(\mu\text{-}OMes^*)\{N(SiMe_3)_2\}]_2$ (**3**) and the base adducts $Mn(OCPh_3)_2(py)_2$ (**4**) (py = pyridine) and $Fe(OCPh_3)_2(THF)_2$ (**5**) are reported. More detailed spectroscopic (^{1}H NMR) studies of **2** and **3** have also been undertaken in order to examine the strength of the –OR bridging in these complexes.

Experimental Section

General Procedures. All reactions were performed under N_2 by using either modified Schlenk techniques or a Vacuum Atmospheres HE 43-2 drybox. Solvents were freshly distilled from Na/K or KOH and degassed three times before use. Commercially available trityl alcohol and 2,4,6-tri-*t*-butylphenol were recrystallized from ether and pentane, respectively. $Mn[N(SiMe_3)_2]_2$[13] and $Fe[N(SiMe_3)_2]_2$[14] were prepared by published procedures. ^{1}H NMR spectra were recorded in toluene-d_8 at 300 MHz on a GE QE-300 spectrometer. Isotropic shifts are reported in parts per million (ppm) and were calculated according to the relationship $(\Delta H/H_0)_{iso} = (\Delta H/H_0)_{obs} - (\Delta H/H_0)_{dia}$ by using the phenol HOMes* as the reference compound. Infrared spectra were recorded in the range 4000–200 cm^{-1} as a Nujol mull between CsI plates using a Perkin-Elmer PE-1430 spectrometer. Magnetic moments were determined by the Evans method.[15]

$[Mn\{O(2,4,6\text{-}t\text{-}Bu_3C_6H_2)\}_2]_2$ (1)[5] and $[Fe\{O(2,4,6\text{-}t\text{-}Bu_3C_6H_2)\}_2]_2$ (2). In a typical experiment, 2.1 g (8 mmol) of $HO(2,4,6\text{-}t\text{-}Bu_3C_6H_2)$ was dissolved in toluene (20 mL). To this a solution was added 1.503 g (4 mmol) of $Mn[N(SiMe_3)_2]_2$ in toluene (30 mL) dropwise. The solution darkened immediately but lightened to an amber color when heated briefly (1 min) with a heat gun. The solution was allowed to stir for a further 3 h and filtered. The volume was reduced under reduced pressure to 10 mL, and the solution was cooled slowly to –25 °C to afford **1** as pale yellow, almost colorless crystals: mp 234–240 °C; yield 1.6 g, 70%. An identical procedure gave **2** as yellow crystals: mp darken >90 °C, 228–235 °C dec; yield 1.51 g, 67%.

$[Fe\{N(SiMe_3)_2\}\{O(2,4,6\text{-}t\text{-}Bu_3C_6H_2)\}]_2$ (3). A 1.05-g (4-mmol) amount of $HO(2,4,6\text{-}t\text{-}Bu_3C_6H_2)$ was dissolved in hexane (20 mL) and added slowly to 1.506 g (4 mmol) of $Fe[N(SiMe_3)_2]_2$ in hexane (10 mL). After several hours of stirring, the dark, olive colored solution was filtered and the volume reduced to 5 mL under reduced pressure. Cooling of this solution overnight in a freezer to –25 °C gave **3** as yellow crystals: mp 155–160 °C; yield 0.4 g, 42%.

$Mn(OCPh_3)_2(py)_2$ (4). A 2.083-g (8-mmol) amount of $HOCPh_3$ was dissolved in pyridine (30 mL). To this solution was added 1.503 g (4 mmol) of $Mn[N(SiMe_3)_2]_2$ via solid addition funnel. The solution turned yellow as the amide dissolved, and a white precipitate formed. Stirring was continued for 6 h. The solution was then heated until the precipitate dissolved. Filtration and cooling slowly to room temperature gave colorless crystals of **4**. The compound may also be recrystallized from hot toluene: yield 2.2 g, 75%.

$Fe(OCPh_3)_2(THF)_2$ (5). A 2.083-g (8-mmol) amount of $HOCPh_3$ was dissolved in THF (30 mL), and 1.506 g (4 mmol) of $Fe[N(SiMe_3)_2]_2$ was added via solid addition funnel. The resultant olive green solution was then stirred for 3 h and reduced in volume to 10 mL under reduced pressure and filtered. Hexane (3 mL) was added, and the solution was cooled slowly in a –20 °C freezer to give colorless crystals of **5**: yield 1.9 g, 66%.

Spectroscopic and Magnetic Data. The UV–vis absorption spectra of compounds **1–5** are almost featureless, and their major characteristic is a gradual rise in absorption toward the higher energy region of the spectrum. Magnetic moments, which were determined in toluene/deuterated toluene mixtures by the Evans method, gave the following values for μ: **1**, 3.6 μ_B; **2**, 3.4 μ_B; **4**, 5.8 μ_B; **5**, 5.2 μ_B. IR data (in cm^{-1}) for **1–3** were as follows: **1**, 1755 w, 1661 w, 1600 w, 1305 m, sh, 1270 m, 1240 m, 142 m, 1183 m, 1152 m, 1115 sh, w, 1605 m, 970 w, 920 sh, w, 885 sh, w, 870 m, 820 m, 808 m, 770 w, 730 br, m, 638 w, 540 m, 518 sh, w, 458 w, 400 w; **2**, 1762 w, 1657 w, 1698 w, 1271 w, 1237 m, 1210 m, 1880 m, 1153 w, 1115 sh, w, 1104 w, 972 w, 918 sh, w, 910 w, 885 sh, w, 870 m, 820 m, 805 m, 772 w, 728 m, 640 w, 555 m, 512 w, 600 w, 404 w; **3**, 1755 w, 1660 w, 1602 w, 1270 sh, m, 1240 m, 1212 m, 1182 m, 1145 sh, m, 1115 sh, w, 1105 w, 1018 w, 970 sh, w, 938 m, 805 w, sh, 842 m, 790 w, sh, 770 w, 750 w, 731 w, 715 w, 610 w, 551 w, 512 w, 465 w, 415 w, 355 m, 253 w. ^{1}H NMR data for **2**: δ 16.2 and –30.2 (*o*-*t*-Bu), 22.6 and –11.1 (*p*-*t*-Bu), 98.5 and 0.3 (*m*-H).

X-ray Crystallographic Studies. X-ray data for **1**, **2**, **4**, and **5** were collected at 130 K with a Syntex $P2_1$ diffractometer equipped with a locally modified LT-1 low-temperature device. Calculations were carried out on a Data General Eclipse computer using the SHELXTL, Version 5, program system. X-ray data for **2** were collected at 130 K with a Syntex R3m/v diffractometer equipped with an Enraf-Nonius universal low-temperature device. Calculations were carried out with the SHELXTL PLUS program system installed on a Microvax 3200 computer. In all cases, scattering factors were from common sources[16] and an absorption correction was appled by using the method described in ref 17.

(9) Sigel, G. A.; Bartlett, R. A.; Decker, D.; Olmstead, M. M.; Power, P. P. *Inorg. Chem.* **1987**, *26*, 1773.
(10) Jones, R. A.; Koschmieder, S. U.; Nunn, C. *Inorg. Chem.* **1988**, *27*, 4527. Two alkyl ligands may also be replaced as in the reaction between $Mn[CH(SiMe_3)_2]_2(THF)$ and HOC_6H_2-2,6-*t*-Bu_2-4-Me: Hitchcock, P. B.; Lappert, M. F.; Leung, W.-P.; Buttrus, N. H. *J. Organomet. Chem.* **1990**, *394*, 57.
(11) McMullen, A. K.; Tilley, T. D.; Rheingold, A. L.; Geib, S. J. *Inorg. Chem.* **1990**, *29*, 2228 and references therein.
(12) Weese, K. J.; Bartlett, R. A.; Murray, B. D.; Olmstead, M. M.; Power, P. P. *Inorg. Chem.* **1987**, *26*, 2409.
(13) Bürger, H.; Wannagat, W. *Monatsh. Chem.* **1964**, *95*, 1009.
(14) Andersen, R. A.; Faegri, K.; Green, J. C.; Haaland, A.; Lappert, M. F.; Leung, W.-P. *Inorg. Chem.* **1988**, *27*, 1782.
(15) Evans, D. F. *J. Am. Chem. Soc.* **1959**, 2005.
(16) *International Tables for X-Ray Crystallography*; Vol. IV. Kynoch Press: Birmingham, England, 1974; Vol. IV.

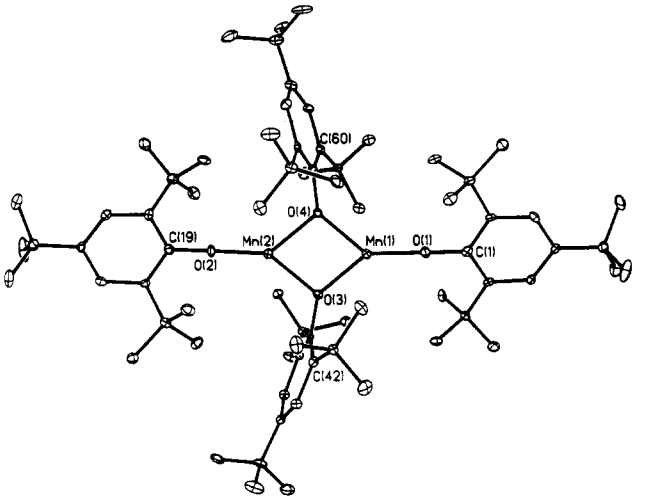

Figure 1. Computer-generated plot of the structure of **1** (30% ellipsoids). H atoms have been omitted for clarity.

X-ray-quality crystals of the title compounds were grown from concentrated solutions in toluene (**1**), hexane (**2** and **3**), pyridine (**4**), or THF/hexane (in the case of **5**). Crystals of **1–5** were removed from the Schlenk tube under a stream of N_2 and immediately covered with a layer of hydrocarbon oil. A suitable crystal was selected, attached with grease to a glass fiber, and immediately placed in the low-temperature nitrogen stream. Some details of the data collection and refinement are given in Table I. Further details are provided in the supplementary material. The structures of **1**, **2**, **4**, and **5** were solved by direct methods and subsequently refined by blocked-cascade least-squares refinement. The structure of **3** was solved by direct methods and refined by full-matrix least-squares refinement. In all cases, hydrogen atoms were included by use of a riding model with C–H distances of 0.96 Å and isotropic thermal parameters equal to 1.2 times that of the bonded carbon. All non-hydrogen atoms were refined anisotropically. Fractional coordinates for important atoms in **1–5** are given in Table II, and selected bond distances and angles are provided in Table III.

Structural Descriptions. [Mn{O(2,4,6-*t*-$Bu_3C_6H_2$)}$_2$]$_2$ (1) and [Fe{O-(2,4,6-*t*-$Bu_3C_6H_2$)}$_2$]$_2$ (2). The crystals of **1** and **2** have similar unit cells. The difference arises from the inclusion of a toluene of crystallization in **1** whereas hexane is included in the lattice of **2**. The structure of these compounds is represented by the drawing of **1** in Figure 1. An illustration of the iron species **2** may be found in ref 18. Both structures are comprised of well-separated, aryloxide-bridged, dimers with no crystallographically imposed symmetry. The structures of **1** and **2** are quite similar. Both possess an essentially planar M_2O_4 core with trigonal-planar geometry for both the metals and bridging oxygens. The metal···metal distances are 3.156 (2) Å for **1** and 3.126 (2) Å for **2**. The bridging metal–oxygen distances for **1** and **2** average 2.050 (8) and 2.016 (8) Å, while the terminal M–O distances are 1.873 (4) Å for **1** and 1.822 (5) Å for **2**. On average, the terminal O–C distances are slightly shorter than the bridging O–C distances in both compounds (1.353 (10) vs 1.387 (9) Å for **1**; 1.365 (18) vs 1.399 (14) Å for **2**). A notable feature of the structures concerns the wide terminal M–O–C angles in both compounds, which can vary widely (178.8 (3) and 167.1 (3)° for **1** vs 161.8 (6) and 151.3 (6)° for **2**). The internal ring angles at the metals average 79.4 (4)° for **1** and 78.3 (3)° for **2** whereas the internal M–O–M angles are 100.7 (2)° for **1** and 101.7 (5)° for **2**. At the metal the external angles are relatively symmetric in both compounds with average values for **1** and **2** of 140.1 (3) and 140.8 (3)°. The angles at the bridging oxygens, however, are very asymmetric and vary from 119.7 (3) to 139.2 (3)° in **1** (average 129.4°) and from 117.4 (5) to 140.4 (5)° for **2** (average 128.9°).

[Fe{N(SiMe$_3$)$_2$}{O(2,4,6-*t*-$Bu_3C_6H_2$)}]$_2$ (3). Compound **3** is illustrated in Figure 2. It can be readily seen that **3** is dimeric with aryloxide bridges and terminal amide groups. The two halves of the dimer are related by a center of symmetry. The Fe_2O_2 core is thus required to be planar. Moreover, the planarity extends to the nitrogen atom, which, like the Fe and O centers, has trigonal-planar geometry. The planes of the phenyl rings of the aryloxide substituents are nearly perpendicular to the Fe_2O_2 plane whereas the amide Si_2N moiety is almost coplanar with the

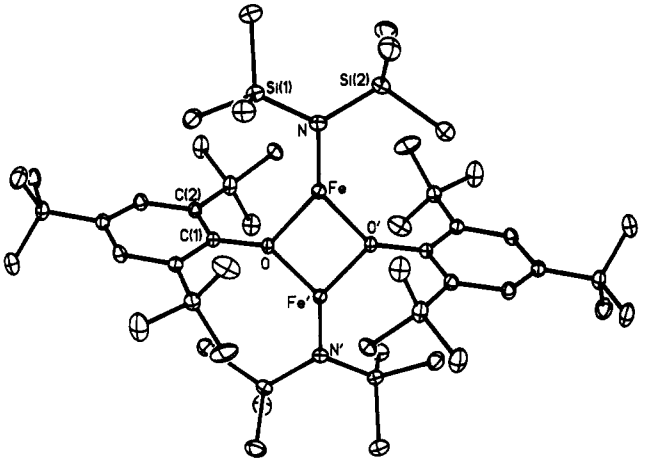

Figure 2. Computer-generated plot of the structure of **3** (30% ellipsoids). H atoms and disordered carbons have been omitted for clarity.

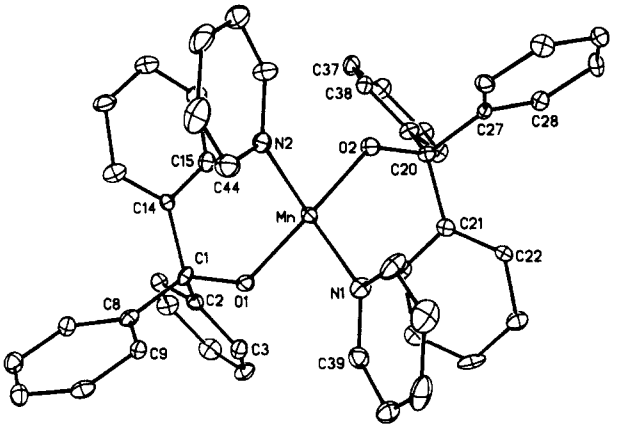

Figure 3. Computer-generated plot of the structure of **4** (30% ellipsoids). H atoms have been omitted for clarity.

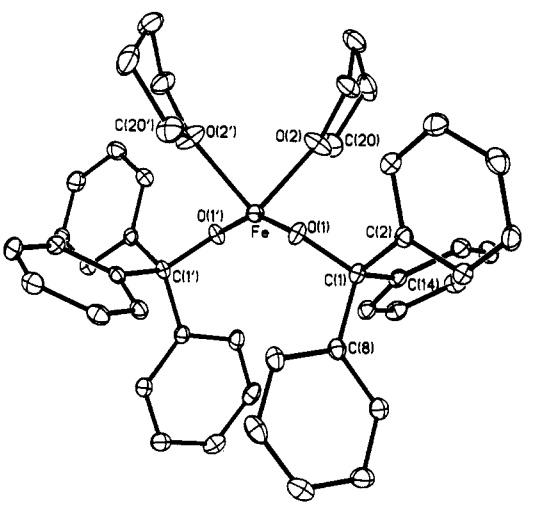

Figure 4. Computer-generated plot of the structure of **5** (30% ellipsoids). H atoms have been omitted for clarity.

Fe_2O_2 array. The Fe–O distances average 2.028 (7) Å, and the Fe–N distance is 1.905 (2) Å. In the Fe_2O_2 core, the internal ring angle at iron is 78.2 (1)°, and the external N–Fe–O angles average 140.9 (3)°. The internal angle at oxygen is 101.8 (1)°. As in the case of **1** and **2** some asymmetry is apparent in the external Fe–O–C angles. The Si–N distance is 1.741 (2) Å, and the Si–N–Si angle is only 117.4 (1)°. The O–C(1) distance is 1.389 (3) Å, and the separation of the iron atoms is 3.147 (2) Å.

Mn(OCPh$_3$)$_2$(py)$_2$ (4). The structure of **4** is illustrated in Figure 3. It is comprised of well-separated monomers with a very irregular four-coordinate arrangement of ligands at the manganese. The Mn–O and Mn–N distances are 1.956 (4) and 2.202 (8) Å. The O(1)–Mn–O(2)

(17) The absorption correction was made by using the program XABS. The program obtains an absorption tensor from F_o–F_c differences: Moezzi, B. Ph.D. Dissertation, University of California, Davis, CA, 1987.

(18) Power, P. P. *Comments Inorg. Chem.* **1989**, *8*, 177.

Table II. Important Atomic Coordinates ($\times 10^4$) and Isotropic Thermal Parameters ($Å^2 \times 10^3$) for **1–5**

	x	*y*	*z*	*U*[a]
		1		
Mn(1)	5029 (1)	1561 (1)	3006 (1)	15 (1)
Mn(2)	6632 (1)	1541 (1)	2076 (1)	16 (1)
O(1)	4025 (3)	1557 (1)	3514 (2)	20 (1)
O(2)	7468 (3)	1503 (1)	1434 (2)	20 (1)
O(3)	5815 (3)	2007 (1)	2517 (2)	14 (1)
O(4)	5865 (3)	1096 (1)	2595 (2)	15 (1)
C(1)	3316 (4)	1549 (2)	3890 (3)	16 (2)
C(19)	8231 (4)	1478 (2)	1110 (3)	17 (2)
C(37)	5991 (4)	2482 (2)	2483 (3)	9 (2)
C(55)	5901 (4)	616 (2)	2519 (3)	14 (2)
		2		
Fe(1)	7331 (1)	1657 (1)	381 (1)	18 (1)
Fe(2)	8412 (1)	1634 (1)	1820 (1)	19 (1)
O(1)	6692 (4)	1669 (2)	−456 (3)	23 (2)
O(2)	8990 (4)	1638 (2)	2671 (3)	23 (2)
O(3)	7791 (5)	1177 (2)	1110 (3)	21 (2)
O(4)	7964 (4)	2110 (2)	1085 (3)	19 (2)
C(1)	6030 (6)	1576 (3)	−1008 (4)	17 (3)
C(19)	9702 (7)	1498 (3)	3162 (5)	24 (4)
C(37)	7782 (7)	663 (3)	1067 (4)	18 (3)
C(55)	8229 (7)	2607 (3)	1185 (4)	17 (3)
		3		
Fe	318 (1)	4142 (1)	6035 (1)	21 (1)
Si(1)	1931 (1)	2027 (1)	7022 (1)	26 (1)
Si(2)	−159 (1)	3225 (1)	8766 (1)	27 (1)
O	726 (2)	4411 (1)	4261 (1)	20 (1)
N	710 (2)	3107 (2)	7288 (2)	24 (1)
C(1)	1356 (2)	3650 (2)	3563 (2)	20 (1)
		4		
Mn	2573 (1)	2334 (1)	2526 (1)	18 (1)
O(1)	1150 (5)	4139 (4)	2112 (2)	23 (2)
O(2)	2617 (5)	528 (4)	2946 (2)	23 (2)
N(1)	3356 (6)	3381 (5)	3087 (2)	24 (2)
N(2)	4856 (6)	1340 (5)	1929 (2)	24 (2)
C(1)	529 (7)	4457 (6)	1538 (3)	18 (3)
C(20)	1821 (7)	206 (6)	3522 (3)	18 (3)
		5		
Fe	5000	4889 (1)	2500	21 (1)
O(1)	3899 (1)	5324 (2)	2055 (1)	24 (1)
O(2)	5153 (1)	3361 (2)	1906 (1)	40 (1)
C(1)	3444 (1)	6114 (2)	1489 (1)	21 (1)

[a] Equivalent isotropic *U* defined as one-third of the trace of the orthogonalized U_{ij} tensor.

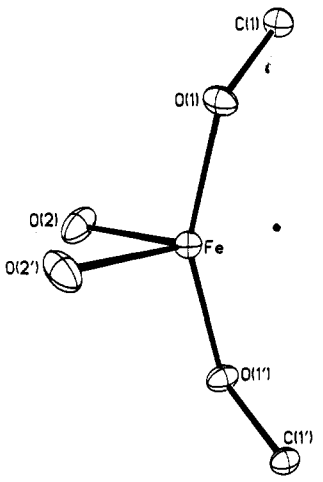

Figure 5. Illustration of the core atoms of **5**, showing the octahedron-derived geometry.

angle, involving the alkoxide substituents, is extremely wide, 140.4 (2)°, whereas the N–Mn–N angle is only 95.6 (2)°. In the alkoxide ligands, the O–C distances are 1.401 (8) Å and the Mn–O–C angles average 131.28 (9)°.

Table III. Important Bond Lengths (Å) and Angles (deg) for **1–5**

Bond Lengths for **1**			
Mn(1)–O(1)	1.879 (4)	Mn(2)–O(4)	2.055 (4)
Mn(1)–O(3)	2.042 (4)	O(1)–C(1)	1.350 (7)
Mn(1)–O(4)	2.046 (4)	O(2)–C(19)	1.356 (7)
Mn(2)–O(2)	1.867 (4)	O(3)–C(37)	1.390 (6)
Mn(2)–O(3)	2.058 (4)	O(4)–C(55)	1.385 (6)

Bond Angles for **1**			
O(1)–Mn(1)–O(3)	141.3 (2)	Mn(1)–O(4)–Mn(2)	100.6 (1)
O(1)–Mn(1)–O(4)	139.0 (2)	Mn(1)–O(1)–C(1)	178.8 (3)
O(2)–Mn(2)–O(3)	142.1 (2)	Mn(1)–O(3)–C(37)	139.2 (3)
O(2)–Mn(2)–O(4)	138.2 (2)	Mn(1)–O(4)–C(55)	136.4 (4)
O(3)–Mn(1)–O(4)	79.6 (1)	Mn(2)–O(2)–C(19)	167.1 (3)
O(3)–Mn(2)–O(4)	79.1 (1)	Mn(2)–O(3)–C(37)	119.7 (3)
Mn(1)–O(3)–Mn(2)	100.7 (1)	Mn(2)–O(4)–C(55)	122.2 (4)

Bond Lengths for **2**			
Fe(1)–O(1)	1.822 (5)	Fe(2)–O(4)	2.024 (6)
Fe(1)–O(3)	2.024 (6)	O(1)–C(1)	1.372 (9)
Fe(1)–O(4)	2.002 (6)	O(2)–C(19)	1.357 (10)
Fe(2)–O(2)	1.822 (6)	O(3)–C(37)	1.395 (10)
Fe(2)–O(3)	2.012 (6)	O(4)–C(55)	1.403 (10)

Bond Angles for **2**			
O(1)–Fe(1)–O(3)	140.8 (3)	Fe(2)–O(2)–C(19)	151.3 (6)
O(1)–Fe(1)–O(4)	140.8 (3)	Fe(1)–O(3)–Fe(2)	101.5 (3)
O(3)–Fe(1)–O(4)	78.4 (2)	Fe(1)–O(3)–C(37)	126.5 (5)
O(2)–Fe(2)–O(3)	141.8 (3)	Fe(2)–O(3)–C(37)	131.3 (5)
O(2)–Fe(2)–O(4)	139.9 (3)	Fe(1)–O(4)–Fe(2)	101.9 (3)
O(3)–Fe(2)–O(4)	78.2 (2)	Fe(1)–O(4)–C(55)	140.4 (5)
Fe(1)–O(1)–C(1)	161.8 (6)	Fe(2)–O(4)–C(55)	117.4 (5)

Bond Lengths for **3**			
Fe–O	2.032 (2)	Si(1)–N	1.741 (2)
Fe–O′	2.023 (2)	Si(2)–N	1.740 (2)
Fe–N	1.905 (2)	O–C(1)	1.389 (3)

Bond Angles for **3**			
O–Fe–N	141.1 (1)	C(1)–O–Fe′	132.0 (2)
O–Fe–O′	78.2 (1)	Fe–N–Si(1)	122.5 (1)
N–Fe–O′	140.7 (1)	Fe–N–Si(2)	120.1 (1)
Fe–O–Fe′	101.8 (1)	Si(1)–N–Si(2)	117.4 (1)
Fe–O–C(1)	125.3 (1)		

Bond Lengths for **4**			
Mn–O(1)	1.956 (4)	O(2)–C(20)	1.401 (7)
Mn–O(2)	1.956 (4)	N(1)–C(39)	1.330 (8)
Mn–N(1)	2.203 (7)	N(1)–C(43)	1.328 (9)
Mn–N(2)	2.201 (5)	N(2)–C(44)	1.347 (11)
O(1)–C(1)	1.400 (8)	N(2)–C(48)	1.337 (9)

Bond Angles for **4**			
O(1)–Mn–O(2)	140.4 (2)	O(2)–Mn–N(2)	94.6 (2)
O(1)–Mn–N(1)	93.2 (2)	N(1)–Mn–N(2)	95.6 (2)
O(1)–Mn–N(2)	111.9 (2)	Mn–O(1)–C(1)	131.2 (4)
O(2)–Mn–N(1)	113.7 (2)	Mn–O(2)–C(20)	131.3 (3)

Bond Lengths for **5**			
Fe–O(1)	1.883 (1)	O(1)–C(1)	1.402 (2)
Fe–O(2)	2.134 (2)		

Bond Angles for **5**			
O(1)–Fe–O(2)	105.0 (1)	O(2)–Fe–O(2′)	93.6 (1)
O(1)–Fe–O(1′)	154.4 (1)	Fe–O(1)–C(1)	130.9 (2)
O(2)–Fe–O(1′)	92.5 (1)		

$Fe(OCPh_3)_2(THF)_2$ (5). The structure of **5** is illustrated in Figure 4. As in the case of **4**, a very irregular four-coordinate geometry at the metal is apparent. The structure consists of well-separated monomers that possess a crystallographically imposed 2-fold axis through the iron atom that bisects the O–Fe–O′ angles. The metal–oxygen(alkoxide) distance is 1.883 (1) Å, and the angle between the alkoxide ligands is 154.4 (1)°. This wide angle may be seen to best advantage in Figure 5. The iron–oxygen(THF) distance is much longer, 2.134 (2) Å, and the angle between the THF ligands is only 93.6 (1)°. For the $-OCPh_3$ group, the C–O distance is 1.402 (2) Å and Fe–O–C angle is 130.9 (2)°.

Discussion

Synthesis and Structures. Compounds **1–5** were synthesized by treatment of the metal amide with the appropriate alcohol according to Scheme I. The reactions proceed smoothly and in

Table IV. Comparison of Important Bond Distances (Å) and Angles (deg) for the Homoleptic Transition-Metal –OR and –OBR_2 Complexes **1**, **2**, and **6**–**10**

	$[Cu\{\mu\text{-}OCH(t\text{-}Bu)_2\}\{OC(t\text{-}Bu)_3\}]_2$ (**8**)[20]	$[Mn(OMes^*)_2]_2$ (**1**)[a]	$[Mn\{OB(2,4,6\text{-}i\text{-}Pr_3C_6H_2)_2\}_2]_2$ (**6**)[21]	$[Fe(OMes^*)_2]_2$ (**2**)[a]	$[Fe(OBMes_2)_2]_2$ (**7**)[21]	$[Co\{OC(C_6H_{11})_3\}_2]_2$ (**9**)[9]	$[Co\{OCPh_3\}_2]_2$ (**10**)[9]
M–O(t)	1.838 (3)	1.873 (4)	1.890 (7)	1.822 (6)	1.821 (5)	1.78 (2)	1.812 (5)
M–O(b)	1.975 (7)	2.050 (4)	2.080 (7)	2.016 (6)	2.007 (5)	1.95 (2)	1.966 (5)
M–O–Br	171.0 (3)	167.1 (3)	168.4 (5)	156.6 (6)	143.9 (5)	145.2 (4)	129.0 (4)
(or C)		178.8 (3)				158.1 (5)	137.1 (4)
C–O or	1.421 (6)	1.350 (6)	1.318 (16)	1.372 (9)	1.354 (11)	1.427 (8)	1.414 (8)
B–O		1.356 (7)	1.358 (14)	1.357 (10)	1.361 (10)	1.447 (8)	1.421 (7)
M···M	3.075 (1)	3.156 (3)	3.094 (5)	3.126 (6)	3.057 (5)	2.904 (5)	2.910 (2)
M–O–M	102.2 (1)	100.6 (1)	96.1 (3)	101.7 (3)	99.3 (2)	96.0 (4)	95.2 (4)
O–M–O	77.8 (1)	79.3 (1)	81.0 (3)	78.3 (2)	80.7 (2)	81.8 (6)	84.6 (4)

[a] This work.

Scheme I

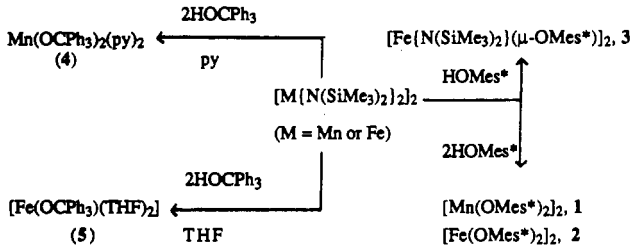

high yield under mild conditions. Moreover, the products are easily purified. The alcoholysis of metal amides is, generally speaking, a superior route to homoleptic transition-metal alkoxides or aryloxides.[1,9,19] This is because the more obvious pathway, involving the treatment of the metal halide with an alkali-metal –OR salt, often affords a product in which the alkali-metal halide salt is either only partially eliminated or forms an integral part of the product.

The compounds **1** and **2** are rare examples of homoleptic –OR derivatives of Mn[1,5,6,20] or Fe.[6] It appears that the species **2** is the first such iron(II) complex to be structurally characterized. The magnetic data for the complexes indicate that the metal centers are high spin and are probably antiferromagnetically coupled. Attempts to grow crystals of the related compounds $[M(OCPh_3)_2]_2$ (M = Mn, Fe) that were suitable for X-ray studies have not been successful thus far. However, Lewis base adducts of these species, as illustrated by compounds **4** or **5**, can be readily obtained. The structures of **1** and **2** may be placed in a broader context by reference to Table IV, which includes data for related Mn and Fe derivatives with boryloxide (–OBR_2) ligands[21] and –OR derivatives of the metals chromium[20] and cobalt.[9] The data exhibit a fairly smooth trend for the Mn, Fe, and Co species. The M–O distances, both terminal and bridging, become shorter across this series, and the M–M separation also decreases. The M–O–C(B) angles in the terminal groups generally become narrower on proceeding to the right. However, it should be emphasized all the M–O–C(B) angles in the complexes are wide, since, with the exception of the Co complex **10**, they are all in excess of 140°. The trend observed for the series of Mn, Fe, and Co complexes is not preserved in the chromium species **8**.[20] Larger M–O angles and M···M separations might have been expected for this metal; however, the structural data for the Cr complex reveal shorter (up to 0.1 Å) M–O bonds than those observed in Mn. The terminal M–O–C angles for the Cr species are very similar to those observed in the Mn complexes. A somewhat narrower M–O–C angle was observed in the species $Cr(OC(t\text{-}Bu)_3)_2{\cdot}LiCl(THF)_2$,[22] which has a terminal Cr–O–C angle of 158.0 (4)° and a Cr–O distance of 1.881 (4) Å. The marginally shorter metal ligand bonds seen in the Cr species **8** are consistent with data[17,23] for the related amide derivatives in which the Cr–N distances are shorter than the corresponding Mn–N bond lengths. Although high-spin Mn(II) and Cr(II) are thought to have very similar ionic radii,[24] it appears that this may not always be the case for low-coordinate –OR or NR_2 derivatives.

An interesting feature of the data in Table IV concerns the comparison of **1** and **2** with the boryloxide complexes **6** and **7**.[21] Clearly, the differences in the structures of the cores between the two pairs of compounds are minor in spite of the replacement of –OMes* by –OBR_2 (R = Mes or 2,4,6-i-$Pr_3C_6H_2$). The substantially different electronic properties of the –OMes* and –OBR_2 ligands appears to have little effect on the lengths of the M–O bonds. One interpretation of this observation is that the M–O bonding is primarily ionic and that the orbital overlap between metal and ligand orbitals play a relatively minor role in determining bond strength. The lack of a strong trend in the M–O–C(B) angles in the complexes in Table IV also supports this view. Wide M–O–C angles in terminal –OR groups have often been interpreted[4,25] on the basis of the involvement of the oxygen lone pairs in π bonding with the metal d orbitals. Provided that the d orbitals are of suitable energy, the strongest π bonding should be observed where the number of d electrons is lowest. In other words π bonding for –OR ligands should decrease from left to right across the transition-metal series. It may be seen in Table IV that M–O–C angles as wide as 158.1 (5)° are observed in the cobalt species **9** whereas very similar angles are observed in the Mn complex **2**. Also, the Cr species **8**, which has three fewer d electrons than the cobalt compound, has a Cr–O–C angle of 171.0 (3)°, which is only ~13° wider than the terminal Co–O–C angle. In other words, an increase of 75% in the number of d electrons effects a relatively small angular change in the terminal oxygen coordination. It is also notable that the terminal M–O–C angle in **1** is marginally wider than that observed in **8** even though **1** has a greater number of d electrons. It could be argued that such comparisons have limited validity, since the sizes of the organic substituents are not consistent across the series. However, it is notable that the pairs of compounds **1** and **6** and **2** and **7** have very similar structural parameters in spite of considerable differences in the size and type of ligand. In addition, the structural data for the Mn_2O_2 core in the complex $[Mn(CH_2CMe_2Ph)(\mu\text{-}OMes^*)]_2$[10] are very similar (Mn···Mn = 3.113 (2) Å, Mn–O (average) = 2.066 (13) Å) to those in Table IV. The same remarks apply to the complex $[Fe\{N(SiMe_3)_2\}(\mu\text{-}OMes^*)]_2$ (**3**), which has Fe–O and Fe···Fe distances (2.028 (7), 3.147 (2) Å) in the Fe_2O_2 core that are not greatly different from those observed for **2**. One other feature of the structure of **3** merits comment. This concerns the relatively narrow Si–N–Si angle of 117.4 (1)° in the terminal amide group. In addition, the Si–N distances are at the longer (1.740 (2) Å) end of the spectrum for those in terminal $-N(SiMe_3)_2$ ligands. These data point to a slightly

(19) Lappert, M. F.; Power, P. P.; Sanger, A. R.; Srivastava, R. C. *Metal and Metalloid Amides*; Ellis-Horwood: Chichester, England, 1980.
(20) Murray, B. D.; Hope, H.; Power, P. P. *J. Am. Chem. Soc.* **1985**, *107*, 169.
(21) Chen, H.; Power, P. P.; Shoner, S. C. *Inorg. Chem.*, preceeding paper in this issue.
(22) Hvoslef, J.; Hope, H.; Murray, B. D.; Power, P. P. *J. Chem. Soc., Chem. Commun.* **1983**, 1438.
(23) Chen, H.; Bartlett, R. A.; Olmstead, M. M.; Power, P. P.; Shoner, S. C. *J. Am. Chem. Soc.* **1990**, *112*, 1048.
(24) Shannon, R. D.; Prewitt, C. T. *Acta Crystallogr.* **1969**, *B25*, 925.
(25) Chisholm, M. H.; Clark, D. C. *Comments Inorg. Chem.* **1987**, *6*, 23.

Table V. Selected Bond Distances (Å) and Angles (deg) for Sterically Crowded Mononuclear Metal Alkoxides

	$Cr(OC_6H_2$-2,6-t-Bu_2-4-$Me)_2(THF)_2$ (**11**)[27]	$Cr(OMes^*)_2(py)_2$ (**12**)[28]	$Mn(OMes^*)_2(MeCN)_2$ (**13**)[28]	$Mn(OCPh_3)_2(py)_2$ (**4**)[a]	$Fe(OCPh_3)_2(THF)_2$ (**5**)[a]	$Co(OCPh_3)_2(THF)_2$ (**14**)[9]	$Zn(OMes^*)_2(THF)_2$ (**15**)[29]
M–OR	1.948 (2)	1.952 (2)	1.910 (6)	1.956 (4)	1.883 (1)	1.872 (2)	1.887 (9)
M–O–C	143.7 (av)	143.4 (1)	179.1 (5)	131.28 (9)	130.9 (2)	129.6 (2)	129.4 (av)
O–M–O	170.44 (9)	180	121.2 (3)	140.4 (2)	154.4 (1)	144.4 (1)	121.7 (3)
L–M–L	177.8 (1)	180	93.8 (4)	95.6 (2)	93.6 (1)	95.5 (2)	94.9 (3)

[a] This work.

increased covalent character in the N–Si and Fe–N bonds in comparison to the terminal group in $[Fe\{N(SiMe_3)_2\}_2]_2$ (N–Si = 1.733 (2) Å and Si–N–Si = 119.1 (2)°).[3] Since the observed narrowing is unlikely to be due to steric effects, it is more probably a result of the replacement of the bridging $-N(SiMe_3)_2$ by OMes*. More ionic bridge bonds would result in a greater partial positive charge at iron, which should result in a lessening of the electron density, which should lead to a narrower Si–N–Si angle.[26]

In the discussion so far the lack of any clear trend in the terminal M–O–C angles has been taken to be indicative of primarily ionic M–O bonding. Another such indicator should be the M–O bond lengths themselves. Some assessment of these lengths can be made by use of Shannon–Prewitt effective ionic radii.[24] Although the lowest metal coordination number featured in these tables of radii is 4, it is possible to extrapolate data for the higher coordination numbers to estimate the effective ionic radii for three coordinate metal ions. For example, in the case of high-spin ion Mn^{2+} the effective ionic radii for six-, five-, and four-coordination modes are 0.83, 0.75, and 0.66 Å. Extrapolation of these figures leads to a value of 0.57 Å for a high-spin three-coordinate Mn^{2+} ion. Similar estimates for high-spin Cr^{2+}, Fe^{2+}, Co^{2+}, and Ni^{2+} lead to approximate values of 0.54, 0.55, 0.50, and 0.48 Å. When the radius of 1.32 Å for two-coordinate OH^- is added to these values, the distances 1.86 (Cr–O), 1.89 (Mn–O), 1.87 (Fe–O), 1.82 (Co–O), and 1.80 Å (Ni–O) are obtained. Although the value for Fe–O is anomalously high, the other predicted distances are in reasonably good agreement with those in Table IV. No dramatic shortening is evident. In short, the data for the terminal M–O bonds provide little support for multiple M–O bonding.

Bond distances and angles in the mononuclear complexes **4** and **5** may also be considered in the light of the possibility of M–O π bonding. Structural data for **4** and **5** and related complexes are presented in Table V.[27,28] Like the compounds in Table IV, the M–OR bond lengths in Table V decrease in the sequence Mn > Fe > Co. However, the M–O bonds in the chromium complexes **11** and **12** are very similar to those seen in the manganese compound **4**. There is very little difference in the M–O–R angles observed in the Mn, Fe, and Co complexes **4**, **5**, and **14**, and the Cr–O–R angles in **11** and **12** are only about 13° wider. The data for the Zn complex **15**,[29] which should have virtually no π bonding since the 3d orbitals are filled, is also very close to those observed for **4**, **5**, and **14**. Thus, in general, the structural data for these complexes do not strongly support the presence of M–O π bonding. The parameters for the manganese species **13**, however, deviate somewhat from the general pattern.[28] In this case the geometry of the Mn–O–R moiety is essentially linear and the Mn–O distance is about 0.04 Å shorter than the Mn–O bond in **4**. The O–M–O angle also differs significantly, being 140.4 (2)° in the case of **4** and 121.2 (3)° in **13**. These differences could be interpreted on the basis of some Mn–O π bonding in **13**. However, it may be argued that the higher crowding in **4**, owing to the presence of pyridine instead of MeCN, gives a wider O–Mn–O angle and longer Mn–O bonds. This could permit the narrower Mn–O–R angles in the case of **4**. In addition, it may be that the differences in size and shape between the $-OCPh_3$ and –OMes* groups require different packing arrangements for compounds, which could account for some of the differences observed between **4** and **13**.

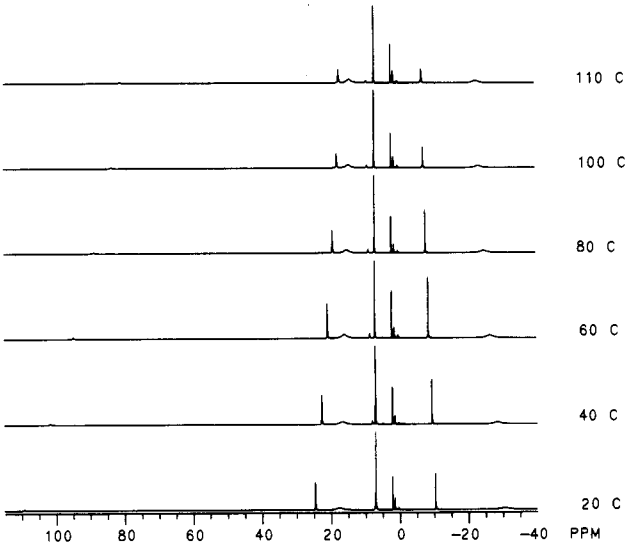

Figure 6. ^1H NMR data for **2** from 20 to 110 °C in C_7D_8.

One of the most interesting features of the complexes in Table V concerns the description of the metal coordination. Clearly, the ligand arrangements in **11**[27] and **12**[28] may be conveniently described as trans square planar. This geometry is probably a result of the high-spin d^4 electron configuration, which (like low-spin[8] configurations) can avoid occupancy of the strongly antibonding $d_{x^2-y^2}$ orbital by adopting the square geometry. The geometries in complexes such as **4**, **5**, and **14** are less easily classified. Because of their four-coordination, there is a strong tendency to describe the geometry as very distorted tetrahedral. However, their very wide (>140°) O–M–O angles and narrow (slightly >90°) L–M–L angles permit an alternative geometrical description that is based upon an octahedron in which two cis apices are missing. This may be illustrated by an alternative view of the iron coordination in **5** as depicted in Figure 5. Obviously, the size difference between the bulky –OR and L groups is responsible for the unusual disposition of the ligands observed in **4**, **5**, and **14**. More subtle effects must also be present. The more regular coordination observed in **13** shows that the angular variation in the M–O–R group also plays a role in determining the metal geometry.

Spectroscopic Studies. Variable-temperature ^1H NMR studies of the iron complexes **2** and **3** were undertaken to establish their dimeric nature in solution and, if possible, to measure the strength of the –OR bridging. No ^1H NMR peaks were observed in the case of the complex **1**, presumably because of the broadness of the resonances. The ^1H NMR spectra of Mn(II) compounds are often difficult to observe owing to slow electron exchange, which causes rapid relaxation. Prior studies[9] in this area have concerned the complex $[Co(OCPh_3)_2]_2$, where it was established that the bridge–terminal exchange barrier was in the range 13.5–14 kcal mol^{-1}. Furthermore, recent measurement on the amide $[Fe\{N(SiMe_3)_2\}_2]_2$ indicated that it had an association energy of ~3

(26) Lappert, M. F.; Power, P. P.; Sanger, A. R.; Srivastava, R. C. *Metal and Metalloid Amides*, Ellis Horwood-Wiley: Chichester, England, 1980.
(27) Edema, J. J. H.; Gambarotta, S.; van Bolhuis, F.; Smeets, W. J. J.; Spek, A. L. *Inorg. Chem.* **1989**, *28*, 1407.
(28) Meyer, D.; Osborn, J. A.; Wesolek, M. *Polyhedron* **1990**, *9*, 1311.
(29) Geerts, R. L.; Huffman, J. C.; Caulton, K. G. *Inorg. Chem.* **1986**, *25*, 1803.

kcal mol^{-1},[30] which indicates much weaker bridging for the amide ligand. The stronger bridging in the alkoxide is consistent with the structure observed for **3** in which the bridging ligand is the aryloxide rather than the amide ligand. The ^{1}H NMR spectrum of **2** in toluene solution at ambient temperature provides a sharp contrast with the amide $Fe[N(SiMe_3)_2]_2$, which is essentially dissociated into monomers under the same conditions. As illustrated in Figure 6, **2** displays six isotropically shifted resonances, which can be assigned to two different sets of OMes* peaks. The relative intensities of the peaks enable assignment into ortho, meta, and para groups. Thus in Figure 6, the peaks observed at 30 °C that correspond to the ortho *t*-Bu groups appear at 17.2 and −29.2 ppm. The para *t*-Bu groups were observed at 23.7 and −10 ppm whereas the meta resonances appeared at 105.7 and 7.5 ppm. Raising the temperature of **2** results in substantial changes in the chemical shift, but no dynamic behavior or coalescence was observed up to 110 °C. It may be concluded that the aryloxo bridges are quite strong and the energy barrier to the coalescence of bridging and terminal ligand resonances in **2** is probably at least 15 kcal mol^{-1}. These data are, of course, consistent with the prior study of $[Co(OCPh_3)_2]_2$ for which relatively strong OR bridging was also observed.[9] One of the major reasons for synthesizing the mixed complex **3** was to enable a facile assignment of the ^{1}H NMR peaks due to the bridging and terminal groups in **2**. Three different ^{1}H NMR spectra of **3**, derived from either (a) mixing equimolar quantities of **2** and $Fe[N(SiMe_3)_2]_2$, (b) adding 1 equiv of HOMes* to $Fe[N(SiMe_3)_2]_2$, (c) dissolving a crystalline sample of **3** in toluene, although they are all very similar, do not present a simple pattern. The spectrum of **3** in toluene-d_8 at 20 °C shows the presence of peaks that are due to **2** and $Fe[N(SiMe_3)_2]_2$. In addition, several other peaks are present, which are probably due to **3** and perhaps a molecule such as $[(Me_3Si)_2NFe(\mu\text{-}OMes^*)_2Fe(\mu\text{-}OMes^*)_2FeN(SiMe_3)_2]$. An equilibrium given by the equation

$$[Fe\{N(SiMe_3)_2\}_2]_2 + [Fe(OMes^*)_2]_2 \rightleftharpoons 2[Fe(\mu\text{-}OMes^*)\{N(SiMe_3)_2\}]_2 \rightleftharpoons \tfrac{1}{2}[Fe\{N(SiMe_3)_2\}_2]_2 + (Me_3Si)_2NFe(\mu\text{-}OMes^*)_2Fe(\mu\text{-}OMes^*)_2FeN(SiMe_3)_2$$

may be occurring in solution. The presence or indeed the structure of the trimetallic species is not established by the data here. However, similar structures have been observed with different ligands in a number of related complexes.[31]

The IR spectra of **1**–**3** were recorded with the objective of determining which bands were associated with the M–O and M–N vibrations. Assignment of the M–O bands in alkoxides and aryloxides is frequently difficult[1] owing to the coupling of the C–O and M–O modes. Comparisons of the data for **1**–**3** with data for HOMes*, $HN(SiMe_3)_2$, and $[Fe\{N(SiMe_3)_2\}_2]_2$ indicate that, in the case of **1**, the bands at 540 and 400 cm^{-1} are probably associated with the M–O bonds. For **2** the corresponding bands appear at 555 and 404 cm^{-1}. The IR spectrum of **3** displays corresponding bands at 550 and 415 cm^{-1}, but a new absorption at 352 cm^{-1} is also apparent. The latter is probably due to the Fe–N stretching mode, since $[Fe\{N(SiMe_3)_2\}_2]_2$ displays a band in the same region at 355 cm^{-1}.[14]

To summarize, the M–O bonding in the compounds described in this paper appears to be primarily ionic. This is in sharp contrast to the higher oxidation state, early-transition-metal complexes, which are thought to have strong M–O π bonding. Quite probably, the high oxidation state of metals in the latter species is primarily responsible for the back-transfer of electron density from oxygen in accordance with the Pauling electroneutrality principle. Such a requirement is present to a much lesser extent in the M^{2+} complexes **1**–**5**.

Acknowledgment. We thank the donors of the Petroleum Research Fund, administered by the American Chemical Society, for financial support.

Supplementary Material Available: Full tables of data collection parameters, atom coordinates, bond distances and angles, hydrogen coordinates and thermal parameters, and anisotropic thermal parameters (43 pages); tables of structure factors (137 pages). Ordering information is given on any current masthead page.

(30) Olmstead, M. M.; Power, P. P.; Shoner, S. C. *Inorg. Chem.*, in press.

(31) Chen, H.; Dias, H. V. R.; Shoner, S. C.; Power, P. P. Unpublished work. This involves the structures of $(Me_3Si)_2NM(\mu\text{-}N(H)Ar)_2M(\mu\text{-}N(H)Ar)_2MN(SiMe_3)_2$ (M = Mg, Mn; Ar = 2,6-*i*-$Pr_2C_6H_3$) and $(Me_3Si)_2NFe(\mu\text{-}SAr)_2Fe(\mu\text{-}SAr)_2FeN(SiMe_3)_2$ (Ar = 2,4,6-*i*-$Pr_3C_6H_2$).